Nonlinear Radiation Pressure Dynamics in an Optomechanical Crystal

Alex G. Krause, Jeff T. Hill, Max Ludwig, Amir H. Safavi-Naeini, Jasper Chan, Florian Marquardt, and Oskar Painter

Phys. Rev. Lett. **115**, 233601 — Published 2 December 2015

DOI: 10.1103/PhysRevLett.115.233601

Nonlinear radiation pressure dynamics in an optomechanical crystal

Alex G. Krause,[1,2] Jeff T. Hill,[1,2,3] Max Ludwig,[4] Amir H. Safavi-Naeini,[1,2,3]
Jasper Chan,[1,2] Florian Marquardt,[4,5] and Oskar Painter[1,2,*]

[1]*Kavli Nanoscience Institute and Thomas J. Watson, Sr., Laboratory of Applied Physics, California Institute of Technology, Pasadena, CA 91125*
[2]*Institute for Quantum Information and Matter, California Institute of Technology, Pasadena, CA 91125*
[3]*Edward L. Ginzton Laboratory, Stanford University, Stanford, CA 94305*
[4]*Institute for Theoretical Physics, Universität Erlangen-Nürnberg, 91058 Erlangen*
[5]*Max Planck Institute for the Science of Light, Günther-Scharowsky-Straße 1/Bau 24, D-91058 Erlangen, Germany*

(Dated: November 6, 2015)

Utilizing a silicon nanobeam optomechanical crystal, we investigate the attractor diagram arising from the radiation pressure interaction between a localized optical cavity at $\lambda_c = 1542$ nm and a mechanical resonance at $\omega_m/2\pi = 3.72$ GHz. At a temperature of $T_b \approx 10$ K, highly nonlinear driving of mechanical motion is observed via continuous wave optical pumping. Introduction of a time-dependent (modulated) optical pump is used to steer the system towards an otherwise inaccessible dynamically stable attractor in which mechanical self-oscillation occurs for an optical pump red-detuned from the cavity resonance. An analytical model incorporating thermo-optic effects due to optical absorption heating is developed, and found to accurately predict the measured device behavior.

Cavity optomechanical systems involving interactions of light and mechanical motion in a mechanically compliant electromagnetic cavity [1] are of interest for precision sensors [2, 3], in nonlinear optics [4, 5], and in the study of macroscopic quantum systems [6, 7]. To lowest order, the mechanical displacement linearly modulates the frequency of the optical resonance in a cavity-optomechanical system. This, however, gives rise to an inherently nonlinear phase modulation, and through radiation-pressure backaction on the mechanical element, yields nonlinear system dynamics [8]. Much of the previous work has focused on the linearized regime where the interaction with the optical field still gives rise to a host of interesting phenomena such as a modified spring constant [9], damping or amplification of the mechanics [10], and EIT-like slow-light effects [11, 12]. Recently, several experiments have pushed into the quantum regime using backaction cooling to bring nanomechanical resonators near their quantum ground state of motion [13, 14].

In this work, we instead demonstrate new features and tools in the nonlinear regime of large mechanical oscillation amplitude. In contrast to the well-known static fixed points of an optomechanical system [15], we are interested here in the dynamic multistability associated with the finite-amplitude mechanical limit cycles that result from radiation pressure dynamic backaction. Previous experimental works have shown that a blue-detuned laser drive can lead to stable mechanical self-oscillations [16–20], and dynamic bistability has been observed for a photothermally driven micromechanical system [21] and in the collective density oscillations of an atomic Bose-Einstein condensate inside a Fabry-Perot cavity [22]. Theoretical predictions, however, indicate that radiation pressure dynamic backaction can lead to an even more intricate, multistable attractor diagram [8]. In the present work we are able to verify the predicted attractor diagram, and further, utilize a modulated laser drive to steer the system into an isolated high-amplitude attractor. This introduces pulsed control of nonlinear dynamics in optomechanical systems dominated by radiation pressure backaction, in analogy to what has been shown recently for a system with an intrinsic mechanical bista-

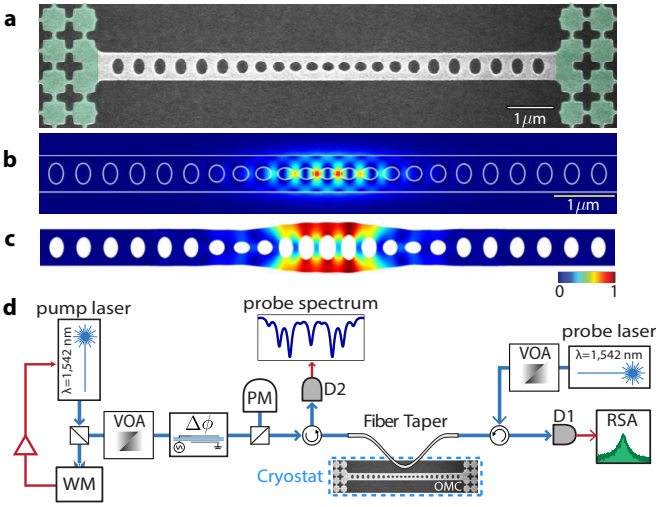

FIG. 1: (a) SEM of the OMC cavity surrounded by phononic shield (green). (b) FEM-simulated electromagnetic energy density of the first-order optical mode. (c) FEM-simulated mechanical mode profile (displacement exaggerated). In (b) the colorscale bar indicates large (red) and small (blue) energy density, whereas in (c) the scale bar indicates large (red) and small (blue) displacement amplitude. (d) Simplified schematic of the experimental setup. WM: wavemeter, $\Delta\phi$: electro-optic phase modulator, D1: pump light detector, D2: probe detector, VOA: variable optical attenuator, PM: power meter. Pump and probe lasers are not mutually coherent to avoid interference effects and we modulate the probe and monitor the detected tone using a lock-in amplifier (not shown).

*Electronic address: opainter@caltech.edu; URL: http://copilot.caltech.edu

bility [23].

We employ a one-dimensional optomechanical crystal (OMC) cavity designed to have strongly interacting optical and mechanical resonances [24]. The OMC structure is created from a free-standing silicon beam by etching into it a periodic array of holes which act as Bragg mirrors for both acoustic and optical waves [25]. A scanning electron micrograph (SEM) of an OMC cavity is shown in Fig. 1a along with finite-element-method (FEM) simulations of the co-localized optical (Fig. 1b) and mechanical (Fig. 1c) resonances. To reduce radiation of the mechanical energy into the bulk, the cavity is surrounded by a periodic 'cross' structure which has a full acoustic bandgap around the mechanical frequency (Fig. 1a, green overlay) [26].

The experimental setup is shown schematically in Fig. 1d. The silicon chip containing the device is placed into a helium flow cryostat where it rests on a cold finger at $T \approx 4$ K (the device temperature is measured to be $T_b \approx 10$ K). Laser light is sent into the device via a tapered optical fiber, which, when placed in the near-field of the device, evanescently couples to the optical resonance of the OMC [27]. A narrow linewidth, frequency tunable pump laser is used to excite and measure the optical and mechanical resonances of the OMC cavity. The transmitted pump light is sent to a high-bandwidth photodetector (D1), which is connected to a real-time spectrum analyzer (RSA) for spectral analysis. Scanning the pump laser frequency and measuring the time-averaged transmitted light intensity yields a resonance dip at $\lambda_c = 1542$ nm for the fundamental optical mode of the device under study in this work. From the spectrum the intrinsic and taper-loaded energy decay rate of the optical resonance is estimated to be $\kappa_i/2\pi = 580$ MHz and $\kappa/2\pi = 1.7$ GHz, respectively. Mechanical motion modulates the phase of the internal optical cavity field, scattering the pump light into motional sidebands which beat with the unscattered pump field on the photodiode [13]. From the microwave spectrum of the measured photocurrent at low pump power we find the breathing mechanical mode to be at frequency $\omega_m/2\pi = 3.72$ GHz with an intrinsic linewidth of $\gamma_i/2\pi = 24$ kHz. These device parameters put our system well into the sideband resolved regime $\kappa/\omega_m \ll 1$.

The interaction between the internal light field and the mechanical motion is given by the interaction Hamiltonian, $H_{\rm int} = \hbar g_0 \hat{a}^\dagger \hat{a} \hat{x}$, where $\hat{a}$ ($\hat{x}$) is the optical (mechanical) field amplitude, and g_0 is the vacuum optomechanical coupling rate. The mechanical displacement expectation is given by $x = x_{\rm zpf}\langle \hat{x} \rangle$, where the zero-point amplitude of the resonator is $x_{\rm zpf} = \left(\hbar/2{\rm m}_{\rm eff}\omega_m\right)^{1/2} = 2.7$ fm (estimated using a motional mass ${\rm m}_{\rm eff} = 311$ fg calculated from FEM simulation). By calibrating the optically-induced mechanical damping versus pump power [13] we find that $g_0/2\pi = 941$ kHz. In the device studied here this vacuum coupling rate is dominated by the photo-elastic component of the radiation pressure force [24].

The classical nonlinear equations of motion for the mechanical displacement (x) and the optical cavity amplitude ($a = \langle \hat{a} \rangle$) are,

$$\ddot{x}(t) = -\gamma_i \dot{x}(t) - \omega_m^2 x(t) + 2\omega_m g_0 x_{\rm zpf} |a(t)|^2, \quad (1)$$

$$\dot{a}(t) = \left[-\frac{\kappa}{2} + i\left(\Delta_L + \frac{g_0}{x_{\rm zpf}} x(t) \right) \right] a(t) + \sqrt{\frac{\kappa_e}{2}} a_{\rm in}, \quad (2)$$

where $a_{\rm in} = \sqrt{P_{\rm in}/\hbar\omega_L}$ is the effective drive amplitude of the pump laser (input power $P_{\rm in}$ and frequency ω_L), $\kappa_e/2$ is the fiber taper input coupling rate, ω_c is the optical cavity resonance frequency, and $\Delta_L \equiv \omega_L - \omega_c$. For self-sustained oscillations, where the motion of the oscillator is coherent on time scales much longer than the cavity lifetime, we can take the mechanical motion to be sinusoidal with amplitude A, $x(t) = A \sin \omega_m t$. The optical cavity field is then given by,

$$a(t) = \sqrt{\frac{\kappa_e}{2}} a_{\rm in} e^{i\Phi(t)} \sum_n i^n \alpha_n e^{in\omega_m t}, \quad (3)$$

where $\Phi(t) = -\beta_m \cos \omega_m t$ and $\alpha_n = J_n(\beta_m) / \left(\kappa/2 + i\left(n\omega_m - \Delta_L\right)\right)$. Here J_n is the Bessel function of the first kind, n-th order, and its argument is the unitless modulation strength $\beta_m = (A g_0) / \left(x_{\rm zpf}\omega_m\right)$. For $\beta_m \ll 1$ only the terms oscillating at the mechanical frequency, ω_m, are appreciable, so the interaction can be linearized, and only the first-order radiation pressure terms are present. However, for $\beta \geq 1$ the higher harmonic terms at each $n\omega_m$ have significant amplitude and backaction force.

The thermal amplitude is too small to enter the nonlinear regime in our devices ($\beta_{\rm th} \approx 0.01$), however, backaction from the pump laser can provide amplification to drive the mechanical resonator into the high-β, nonlinear regime. The resulting mechanical gain spectrum in the amplitude-detuning plane (the attractor diagram) can be solved for by calculating the energy lost in one mechanical cycle ($P_{\rm fric} = {\rm m}_{\rm eff}\gamma_i \langle \dot{x}^2 \rangle$) and comparing it to that gained (or lost) from the optical radiation force ($P_{\rm rad} = \left(\hbar g_0/x_{\rm zpf}\right) \langle |\hat{a}|^2 \dot{x} \rangle$) [8] . Figure 2a shows a plot of the gain spectrum for the parameters of the device studied here with a laser pump power of $P_{\rm in} = 151$ μW. Imposing energy conservation, $P_{\rm rad}/P_{\rm fric} = +1$, yields the steady-state solution contour lines. Although the entire contour is a physical solution, the equilibrium is only stable when the power ratio decreases upon increasing the mechanical amplitude, $\frac{\partial}{\partial \beta} \frac{P_{\rm rad}}{P_{\rm fric}} < 0$ (i.e. stability is found at the 'tops' of the contours) [8]. At higher powers (black contours) we see that for many laser detunings there are several stable mechanical-amplitude solutions demonstrating the presence of dynamic multistability.

In the device studied here there is a thermo-optic frequency shift of the optical cavity caused by heating due to intracavity optical absorption. The thermal time constant of the device structure is slow relative to the optical cavity coupling rate, but fast compared to the laser scan speed. Absorption heating can thus be modeled as a shift of the laser detuning proportional to the average intra-cavity photon number ($\bar{n}_a$), $\Delta_L = \Delta_{L,0} + c_{\rm to}\bar{n}_a$, where $\Delta_{L,0}$ is the bare laser-cavity detuning in absence of thermo-optic effects. The per photon thermo-

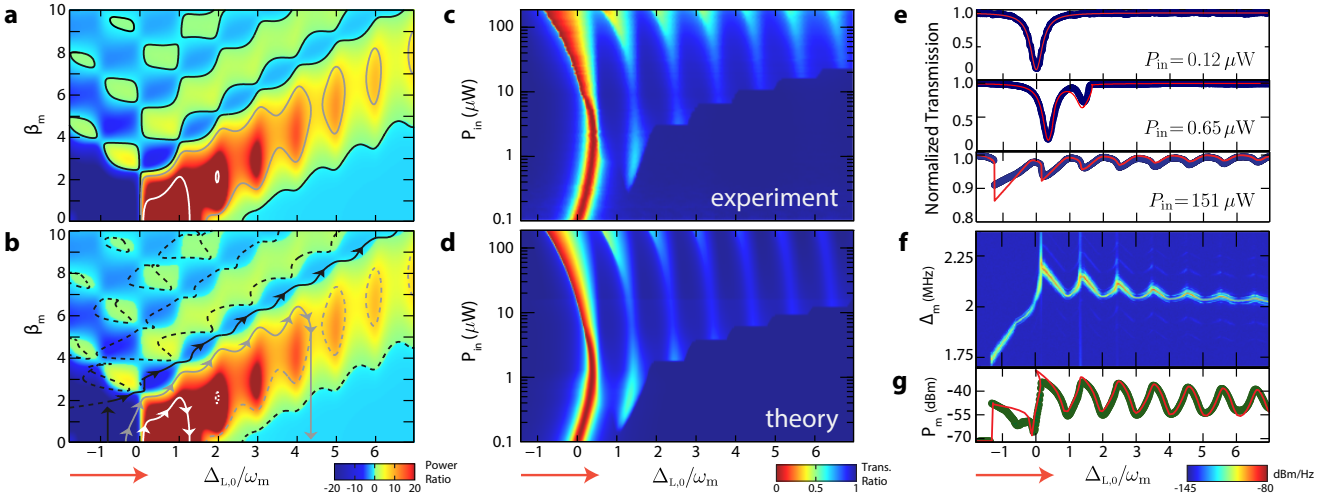

FIG. 2: (a) Calculated gain spectrum for the OMC in the amplitude-detuning plane. Color scale indicates $(P_{\rm rad}/P_{\rm fric}-1)$ at $P_{\rm in}=151\ \mu$W. Solid line curves indicate power-conserving solution contours at selected input powers: 0.65 μW (white), 6.5 μW (grey), 151 μW (black). (b) Same as (a) with contours now shifted by estimated thermo-optic effects (the intensity plot of the gain is left unshifted for reference). Solid line curves indicate the path taken by the mechanical oscillator during a slow laser frequency sweep. Dashed lines are contours which are either unstable or unreachable using this method. (c) Image plot of the measured optical transmission spectrum versus laser detuning and power. The wavelength scan rate ($\sim$ 300 GHz/s) is much slower than the internal dynamics of the optomechanical system. (d) Image plot of the theoretically calculated transmission spectra including thermo-optic shifts and a slow drift in the optical resonance frequency over the course of the measurement from low to high power. Spectra in (c) and (d) are normalized at each power level. (e) Plot of the normalized optical transmission from scans in (c) at $P_{\rm in}=0.12\ \mu$W (top), 0.65 μW (center), 151 μW (bottom). Blue points are measured data and the red curves are the theoretical model. (f) Power spectral density of transmitted pump photocurrent near the mechanical frequency for $P_{\rm in}=151\ \mu$W. (g) Total integrated power of spectra in (f). Measured data are plotted as green circles, with the theoretical model (up to a scale factor) shown as a solid red curve. The red arrow in each plot indicates the laser scan direction.

optic frequency shift of the optical cavity is measured to be $c_{\rm to}/2\pi=-216$ kHz. Including this effect, the shifted contours are shown in Fig. 2b as a function of the bare detuning $\Delta_{L,0}$. The solid lines with arrows indicate the expected path traversed by the mechanical resonator during a slow laser scan from lower to higher laser frequency (left to right) at each power. The dashed lines are contours that are either unstable, or unreachable by this adiabatic laser sweep. Note that while thermo-optic frequency shifts can be up to $10\omega_m$ on resonance, the contours traced out by the laser sweep are only slightly shifted as the laser never reaches the cavity resonance due to the thermo-optic bistability.

In Fig. 2c-g we explore the lowest-lying contour of the attractor diagram by measuring the optical transmission as the pump laser is tuned from red to blue across the optical cavity resonance with different fixed optical input powers. At low optical input powers ($P_{\rm in}<0.3\ \mu$W), only a single resonance dip associated with the bare optical cavity is observed. Upon increasing the laser power, radiation pressure backaction amplifies the thermal motion of the mechanical resonator beyond threshold and into a large amplitude state. When this occurs a large fraction of the intra-cavity photons are scattered, resulting in additional transmission dips near each detuning $\Delta_L=n\omega_m$. Physically, mechanical oscillations at the n-th sideband detuning are generated by a multi-photon gain process involving n photon-phonon scattering events. This stair-step behavior is seen in the measured transmission spectrum of both Fig. 2c and Fig. 2e. The theoretically calculated spectra for our measured device parameters are shown in Fig. 2d, showing good agreement with the measured spectra after including thermo-optic effects. Figure 2f shows the microwave noise power spectrum at the highest measured input power ($P_{\rm in}=151\ \mu$W), indicating a significant optical spring effect (~ 2 MHz) with complicated detuning dependence. Figure 2g shows the integrated power in the first motional sideband versus detuning. The discrepancy between the measured and modeled curve (solid red line) near the largest transmission dip at the highest power is likely due to the effects of nonlinear optical absorption at high intra-cavity photon numbers which is not included in our model.

It is readily apparent from Fig. 2a that at large optical powers (black contour) there are also a number of isolated attractor contours at higher oscillation amplitudes. Here we utilize external time-dependent driving of the mechanical mode to explore the lowest-lying isolated attractor on the red side of the optical cavity ($\Delta_L<0$), where the linearized theory predicts only damping of the mechanical mode. An electro-optic modulator (EOM) is utilized to phase-modulate the incoming light field (see Fig. 1d), resulting in an oscillating force inside the cavity which drives the mechanical resonator towards higher amplitudes. The experimental sequence is displayed in Fig. 3a. We start with the pump laser switched on at a power of $P_{\rm in}=43\ \mu$W, the laser detuned to the red side of the cavity resonance, and the phase modulation off ($\beta_{\rm EOM}=0$), which

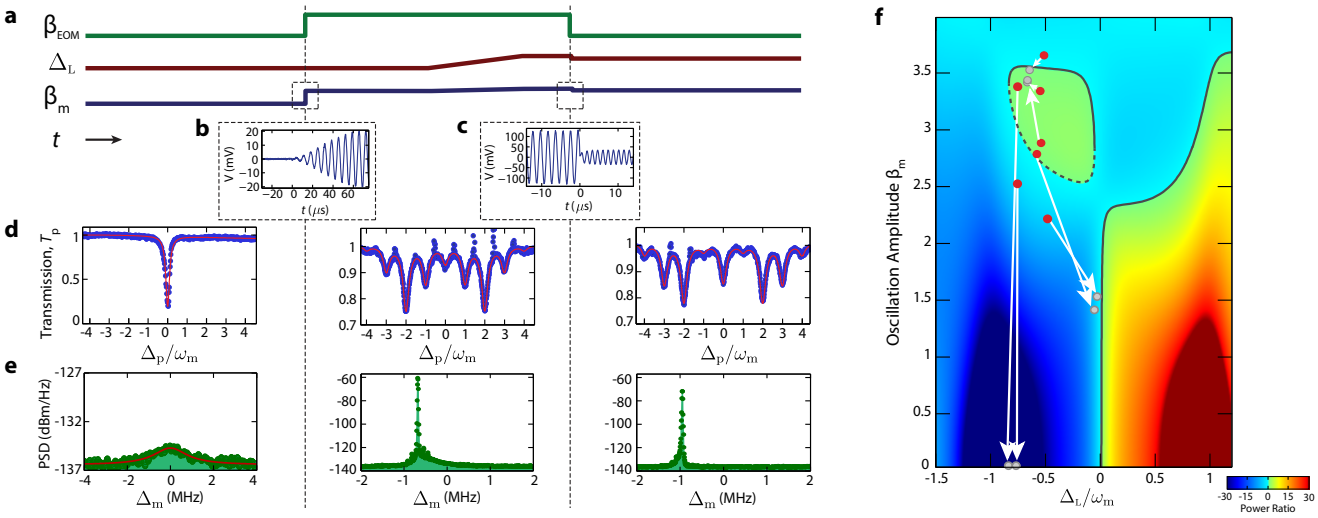

FIG. 3: (a) Schematic showing the state preparation and measurement sequence used to explore the higher lying attractors. (b) Measured time-domain signal of one quadrature of the transmitted pump photocurrent during the turn-on of the EOM drive ($t = 0$). The signal is mixed down from the mechanical resonance frequency at 3.7 GHz to 150 kHz. (c) Measured transmitted pump photocurrent (mixed down to 500 kHz) during the turn-off of the EOM drive modulation. Here we show a case where the system remained trapped in the high-amplitude state. (d) Transmission scans of the counter-propagating probe laser during each sequence of the measurement. Blue points are measured data and red curves are fits to the data. (e) Mechanical power spectrum (green points) during each sequence of the measurement. (f) Plot of the normalized gain spectrum in the detuning-amplitude plane with overlaid stable solution contour (black solid curve) at $P_{\rm in} = 43\ \mu$W. Color scale is the power ratio, $(P_{\rm rad}/P_{\rm fric} - 1)$. Dashed black curve indicates unstable portion of contour. Red data points indicate initial (β_m, Δ_L) and grey data points indicate the final values. White arrows connect initial/final pairs but do not indicate the actual path taken by the system.

initializes the mechanical resonator into a cooled thermal state with $\beta_m \approx 0$. The EOM phase modulation is then turned on which rings up the mechanical resonator. Following ring-up, the pump laser is tuned to a starting detuning of Δ_L, completing the initialization sequence. Finally, the modulation is switched off ($\beta_{\rm EOM} \to 0$) and the system relaxes into a final mechanical oscillation amplitude and laser-cavity detuning.

A time domain signal of the modulated transmitted light field is measured at each stage of the above procedure by mixing down the measured photocurrent on the RSA (see Figs. 3b and 3c). In order to determine the mechanical amplitude β_m and true laser-cavity detuning Δ_L, we use a second counter-propagating weak optical probe laser of frequency ω_p to obtain a cavity spectrum (see Fig. 1d and caption for details). When the mechanical amplitude is large ($\beta_m \gtrsim 1$) the standard single resonance dip is transformed into a multi-featured spectrum with resonance dips at the motional sidebands, $\Delta_p \equiv \omega_p - \omega_c = n\omega_m$ (see panels in Fig. 3d). A fit to the probe spectrum is performed using Eq. 3, with β_m and ω_c as free parameters. A plot of the microwave power spectrum of the photodetected transmitted pump light is also plotted in Fig. 3e, showing the linewidth narrowing and frequency shift in the mechanical resonator as it transitions between different states. Repeating the measurement for different initial states and recording the resulting final states reveals the flow in the underlying attractor diagram. For clarity, only a representative subset of the 38 measurement runs performed is presented in Fig. 3f. We find that for a narrow range of initial conditions (occurring in 22 of the 38 measurement runs), after the modulation is switched off the system remains trapped close to the predicted top of the higher amplitude attractor at $\beta_m \approx 3.5$ and $\Delta_L/\omega_m \approx -0.7$. For more negative initial detunings or lower initial mechanical amplitudes, the system relaxes into the trivial low-amplitude state or gets caught on the lowest-lying contour explored in Fig. 2 (for detunings $\Delta_L/\omega_m > -0.5$ the system could not be stably initialized due to the thermo-optic effect).

The results presented here represent an initial exploration of the nonlinear attractor diagram of an optomechanical system where the dominant nonlinearity is that of the radiation pressure interaction. Due to the limited drive amplitude of the electro-optic modulator used in this work ($\beta_{\rm EOM} \lesssim 3.5$), we are limited to exploring only the lowest red-side attractor. With the ability to apply larger drives, or to rapidly detune the laser, it should be possible to reach higher-lying islands, and more fully explore the attractor diagram shown in Fig. 2a. Further understanding of the latching effects in these measurements should also pave the way to exploiting them for use in metrology experiments as the dynamics that govern whether the oscillator stably latches into an attractor can be a very sensitive function of the oscillator's displacement [8], thus yielding a precise measurement of the oscillator's environment or state. This latching also allows for systems with memory due to the hysteretic nature of the nonlinearity, as in [23, 28–31]. Finally, in future devices where the optomechanical coupling rate is larger, these same nonlinearities can lead to quantum mechanical effects which have thus far only been explored theoretically [32].

This work was supported by the DARPA ORCHID and MESO programs, the Institute for Quantum Information and Matter, an NSF Physics Frontiers Center with support of the Gordon and Betty Moore Foundation, the AFOSR through the "Wiring Quantum Networks with Mechanical Transducers" MURI program, and the Kavli Nanoscience Institute at Caltech. F.M. acknowledges an ERC Starting Grant OPTOMECH, ITN cQOM.

[1] T. J. Kippenberg and K. J. Vahala, Science **321**, 1172 (2008).
[2] A. G. Krause, M. Winger, T. D. Blasius, Q. Lin, and O. Painter, Nature Photonics **6**, 768 (2012).
[3] K. Srinivasan, H. Miao, M. T. Rakher, M. Davanco, and V. Aksyuk, Nano Letters **11**, 791 (2011).
[4] J. T. Hill, A. H. Safavi-Naeini, J. Chan, and O. Painter, Nature Communications **3**, 1196 (2012).
[5] A. H. Safavi-Naeini, S. Grblacher, J. T. Hill, J. Chan, M. Aspelmeyer, and O. Painter, Nature **500**, 185 (2013).
[6] Y. Chen, Journal of Physics B: Atomic, Molecular and Optical Physics **46**, 104001 (2013).
[7] W. Marshall, C. Simon, R. Penrose, and D. Bouwmeester, Physical Review Letters **91**, 130401 (2003).
[8] F. Marquardt, J. G. E. Harris, and S. M. Girvin, Physical Review Letters **96**, 103901 (2006).
[9] M. Eichenfield, R. Camacho, J. Chan, K. J. Vahala, and O. Painter, Nature **459**, 550 (2009).
[10] Q. Lin, J. Rosenberg, X. Jiang, K. J. Vahala, and O. Painter, Physical Review Letters **103**, 103601 (2009).
[11] A. H. Safavi-Naeini, T. P. M. Alegre, J. Chan, M. Eichenfield, M. Winger, Q. Lin, J. T. Hill, D. E. Chang, and O. Painter, Nature **472**, 69 (2011).
[12] S. Weis, R. Rivire, S. Delglise, E. Gavartin, O. Arcizet, A. Schliesser, and T. J. Kippenberg, Science **330**, 1520 (2010).
[13] J. Chan, T. P. M. Alegre, A. H. Safavi-Naeini, J. T. Hill, A. Krause, S. Grblacher, M. Aspelmeyer, and O. Painter, Nature **478**, 89 (2011).
[14] J. D. Teufel, T. Donner, D. Li, J. W. Harlow, M. S. Allman, K. Cicak, A. J. Sirois, J. D. Whittaker, K. W. Lehnert, and R. W. Simmonds, Nature **475**, 359 (2011).
[15] A. Dorsel, J. D. McCullen, P. Meystre, E. Vignes, and H. Walther, Phys. Rev. Lett. **51**, 1550 (1983).
[16] T. Carmon, H. Rokhsari, L. Yang, T. J. Kippenberg, and K. J. Vahala, Physical Review Letters **94**, 223902 (2005).
[17] H. Rokhsari, T. Kippenberg, T. Carmon, and K. Vahala, Optics Express **13**, 5293 (2005).
[18] T. J. Kippenberg, H. Rokhsari, T. Carmon, A. Scherer, and K. J. Vahala, Physical Review Letters **95**, 033901 (2005).
[19] K. Karrai, I. Favero, and C. Metzger, Physical Review Letters **100**, 240801 (2008).
[20] T. Carmon, M. C. Cross, and K. J. Vahala, Physical Review Letters **98**, 167203 (2007).
[21] C. Metzger, M. Ludwig, C. Neuenhahn, A. Ortlieb, I. Favero, K. Karrai, and F. Marquardt, Physical Review Letters **101**, 133903 (2008).
[22] F. Brennecke, S. Ritter, T. Donner, and T. Esslinger, Science **322**, 235 (2008).
[23] M. Bagheri, M. Poot, M. Li, W. P. H. Pernice, and H. X. Tang, Nature Nanotechnology **6**, 726 (2011).
[24] J. Chan, A. H. Safavi-Naeini, J. T. Hill, S. Meenehan, and O. Painter, Applied Physics Letters **101**, 081115 (2012).
[25] M. Eichenfield, J. Chan, R. M. Camacho, K. J. Vahala, and O. Painter, Nature **462**, 78 (2009).
[26] T. P. M. Alegre, A. Safavi-Naeini, M. Winger, and O. Painter, Optics Express **19**, 5658 (2011).
[27] C. P. Michael, M. Borselli, T. J. Johnson, C. Chrystal, and O. Painter, Optics Express **15**, 4745 (2007).
[28] M. I. Dykman and M. A. Krivoglaz, Soviet Journal of Experimental and Theoretical Physics **50**, 30 (1979).
[29] I. Siddiqi, R. Vijay, F. Pierre, C. M. Wilson, M. Metcalfe, C. Rigetti, L. Frunzio, and M. H. Devoret, Physical Review Letters **93**, 207002 (2004).
[30] I. Siddiqi, R. Vijay, F. Pierre, C. M. Wilson, L. Frunzio, M. Metcalfe, C. Rigetti, R. J. Schoelkopf, M. H. Devoret, D. Vion, et al., Physical Review Letters **94**, 027005 (2005).
[31] P. Jung, S. Butz, M. Marthaler, M. V. Fistul, J. Leppkangas, V. P. Koshelets, and A. V. Ustinov, Nature Communications **5** (2014).
[32] M. Ludwig, B. Kubala, and F. Marquardt, New Journal of Physics **10**, 095013 (2008).